Research Square

Preprints are preliminary reports that have not undergone peer review.
They should not be considered conclusive, used to inform clinical practice,
or referenced by the media as validated information.

Machine Learning–Based Computational Framework for Graphene–Silicon Twin-Port Band-Notched Wideband Antenna in Optical Regime

Goutam DATTA
University of Petroleum and Energy Studies
Asha VERMA
Pranveer Singh Institute of Technology
Pooja Singh
poojasinghgalgotiya@gmail.com

Galgotias University
Sreedhar Jadapalli
Vignana Bharathi Institute of Technology
Neha K. Saini
Government Engineering College

Research Article

Keywords: Graphene Material, Dielectric Antenna, MIMO Antenna, Machine learning

Posted Date: September 30th, 2026

DOI: https://doi.org/10.21203/rs.3.rs-8345696/v1

License: This work is licensed under a Creative Commons Attribution 4.0 International License.
Read Full License

Additional Declarations: No competing interests reported.

Machine Learning–Based Computational Framework for Graphene–Silicon Twin-Port Band-Notched Wideband Antenna in Optical Regime

Goutam Datta[1], Asha Verma[2], Pooja Singh[3*], Sreedhar Jadapalli[4], Neha K. Saini[5]
[1]*School of Computer Science, University of Petroleum and Energy Studies (UPES), Dehradun, Uttarakhand, India*
[2]*Electronics and Communication Engineering, Pranveer Singh Institute of Technology, Kanpur, Uttar Pradesh, India*
[3]*Computer Science and Engineering, Galgotias University, Greater Noida, Uttar Pradesh. India*
[4]*Department of Electrical and Electronics Engineering, Vignana Bharathi Institute of Technology, Hyderabad, India*
[5]*Department of Electronics & Communication India Engineering, Government Engineering College, Dahod, Gujarat, India*
gdatta1@yahoo.com, verma.asha.asha@gmail.com, poojasinghgalgotiya@gmail.com, sreedharmtech@gmail.com, ec.nehasaini@gmail.com
[*]*Corresponding Author: Pooja Singh*

Abstract: A 2-port graphene-silicon-built THz antenna is planned and examined in this communication. Aperture feeding and air cavities in silicon dielectric are used to achieve wideband features i.e. 2.35-3.8 THz. Three unique features of designed antenna are: (i) circular metallic rings added with printed line to notched the frequency band, i.e., 2.75-3.15 THz; (ii) Deep neural network (DNN) and Random Forest (RF) are applied to guess |S11| parameter of the designed radiator; and (iii) presence of DGS reduces the coupling below -25 dB. Graphene layering assists in providing frequency tunability qualities to the planned antenna. CST and HFSS EM software confirm the final outcome that the planned antenna works in between 2.2-2.65 THz and 3.3-3.7 THz. A Stable radiation feature and good multi-port parameters confirm its applicability for mobile communication in the THz regime.

Keywords: Graphene Material, Dielectric Antenna, MIMO Antenna, Machine learning

1. Introduction

Upcoming wireless communication applications and systems are pushing the limits of data rates. Terabit-per-second data speeds are possible with the THz spectrum, which is essential for the needs of the future generation [1]. The creation of effective THz antennas is essential to overcoming obstacles at these frequencies, such as significant path loss and air absorption. Researchers are investigating various antennas, including graphene-built and dielectric antennas [2, 3]. These antennas offer adaptability and high radiation efficiency. Antenna designers in the THz range have also had to address the issue of intricate antenna construction meshing, which causes the simulator to take a long time to provide results. ML approaches may be used to tackle this issue [4].

The scientific community is heavily interested in multi terminal antennas in the THz spectrum. Gaurav developed a 2-terminal ceramic antenna that performs between 1.73 THz and 1.83 THz and has a separation value over 20 dB [5]. Together with other researchers, Rubani provided a 2-terminal silver-built antenna with an isolation of roughly 17 dB that performs throughout the 8.69–8.89 THz region [6]. A 2-terminal tree-shaped graphene radiator with an isolation over 25 dB and good performance throughout the 0.25–0.72 THz region was suggested by Babu et al. [7]. Vamsi designed a 2-terminal graphene-based radiator that runs in 4.68–4.88 THz region. The isolation achieved is over 30 dB [8]. Vishwnath et al. built an adjustable 2-terminal hybrid radiator active in the 4.25–4.85

THz region [9]. Ali developed a 2-terminal graphene radiator with a useful spectrum of around 0.12 THz. To reduce the value of ECC, it makes use of the beam twisting idea [10]. Numerous studies also examine radiator modelling in the microwave space using ML approaches. Zheng et al. employed an SVM-based ML architecture to enhance the |S11| of the printed radiator [11]. Sharma et al. utilized ML techniques to anticipate the outcomes of T-shaped printed radiators [12]. Ranjan et al. employed and compared various ML algorithms to boost the functioning of a UWB printed radiator [13]. A KBNN was applied to calculate the dielectric radiator's |S11| by Srivastava et al. [14]. Using ML approaches for antenna design in the THz region has many advantages due to the high time requirements of EM simulators.

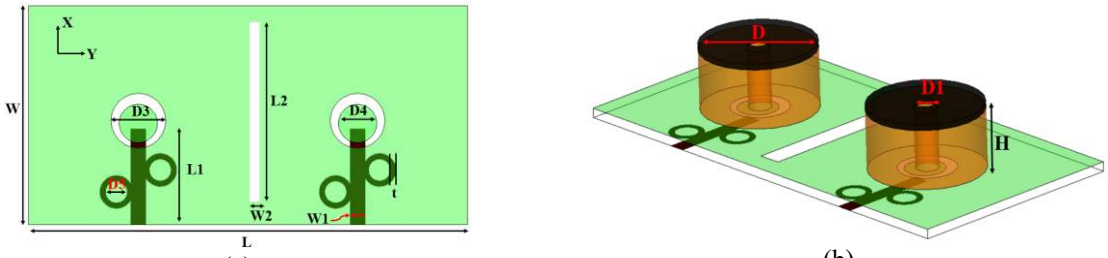
This paper plans and simulates the 2-port silicon-graphene antenna in the THz region. First, aperture stimulation along with the air cavity inside the silicon dielectric helps to wideband features. Circular silver rings in addition to a printed line band notched in between 2.75 THz and 3.15 THz. Graphene coating adds the frequency tunability feature. DGS improves the isolation value between the antenna terminal. This article is segmented into various parts: (a) antenna layout; (b) antenna investigation; (c) $|S_{11}|$ prediction using ML; (d) final outcomes; and (e) conclusion.

2. Antenna Layout

Fig. 1 shows the setup for the planned multi-terminal aerial. A Modified ring-formed slot stimulated silicon ring dielectric rod (εr=11.2) is the planned 2-terminal aerial. Its design uses the SiO_2 dielectric base (εr=3.9). Its thickness is estimated to be 1.6 µm. Graphene, which has a depth of 0.34 nm, is applied on Si-dielectric to alter the antenna's attributes. For the conducting parts of the antenna, such as the ground and microstrip line with circular rings, silver is used. Drude's strategy [15] can precisely express the dispersive nature of the antenna. It is expressed as follows:

$$\varepsilon_{Ag} = \varepsilon_0 \left[\varepsilon_r - \frac{f_1^2}{\{f + if_2\}} \right] \quad (1)$$

The symbols "f1" and "f2" in the equation above stand for plasma and collision frequency, respectively. For silver used in THz antennas, the potential values of "f1" and "f2" are 4.25 THz and 2265 THz, respectively [15]. Details on the optimal antenna size are provided in Table 1.



(a) (b)

Fig. 1 Two-Terminal THz Antenna Layout (a) Slot and printed line as stimulator (b) Adjacent view of radiator

Table-1 Optimal Sizes of various antenna parameters of Planned THz Radiator

Parameters	Size (µm)	Parameters	Size (µm)
W	44.0	D	18.0
L	82.0	D1	2.5
L1	21.5	H	8.0
D5	3.0	L2	38.0
W2	1.5	W1	2.5
t	0.5	D4	5.95
D3	7.2	H_S	1.6

3. Antenna Analysis

This segment provides the detailed examination of the planned radiator using HFSS EM software. Fig. 2 presents the $|S_{11}|$ graph with different changes in the planned radiator: (a) without any dielectric radiator; (b) circular aperture coupled cylindrical dielectric rod; (c) circular aperture coupled ring dielectric rod; (d) ring aperture coupled ring dielectric; and (e) asymmetric ring aperture coupled ring dielectric. Some observations are found from Fig. 2: (i) entire operating regime is because of silicon dielectric; (ii) ring dielectric improves the impedance bandwidth; and (iii) asymmetric ring aperture stimulation provides dual resonance with wider impedance bandwidth due to reduction in capacitive effect. Fig. 3 presents $|S_{11}|$ graph in the existence/non-existence of a dual circular ring with a printed line. It can be seen from Fig. 3 that the addition of circular rings with printed line rejected the frequency band in between 2.75 and 3.15 THz. Fig. 4 shows the E-field lines used to determine the sources of resonances at 2.5 THz and 3.5 THz. It can be perceived from Fig. 4 that $HEM_{11\delta}^{y}$ and $HEM_{11\delta}^{x}$ are accountable for resonances at 2.5 THz and 3.5 THz respectively [16]. This can also be confirmed with the help of the mathematical equation given below [17]:

$$f_r = \frac{9.481 \times 10^8}{\pi D\sqrt{\varepsilon_{Si}}}\left\{0.25 + 0.34\left(\frac{D}{2H}\right) + 0.19\left(\frac{D}{2H}\right)^2\right\} \quad (2)$$

In eqn. (2), 'D' and 'H' represents the diameter and height of ring dielectric rod. 'ε_{Si}' denotes the permittivity of Silicon dielectric rod. After placing all the values, the resonance is found to be 2.75 THz, which is close to simulated value.

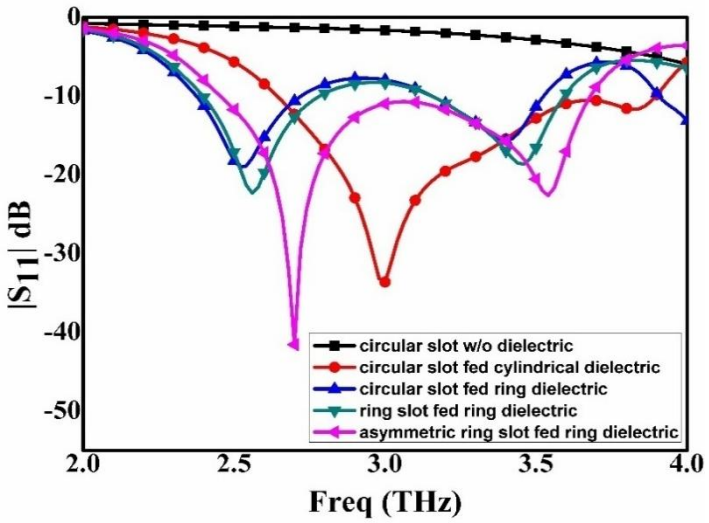


Fig. 2 Graph of $|S_{11}|$ with different changes in single terminal radiator

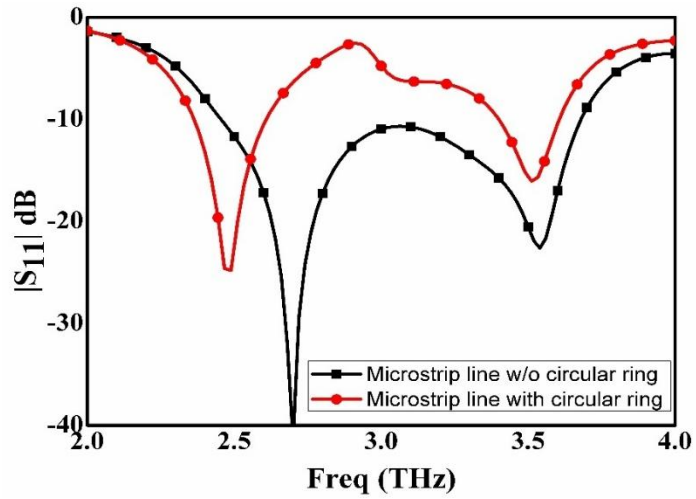
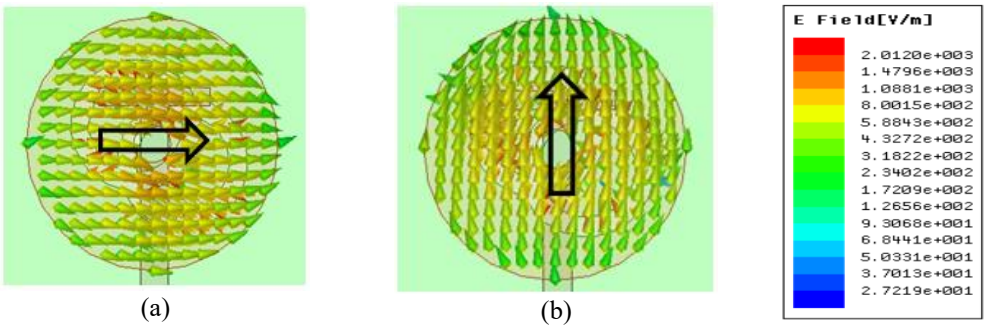


Fig. 3 Graph of $|S_{11}|$ with and without circular rings in printed line



(a) (b)

Fig. 4 E-field lines on ring dielectric rod (a) 2.5 THz (b) 3.5 THz

A minimal coating of graphene is layered with ceramic to render the radiator frequency reconfigurable. The intraband conductance of the graphene film is influenced by fluctuations of its chemical potential (μc), which may be understood using the following algebraic connection [8]:

$$\sigma_{intra}(\omega,\mu_c,\Gamma,T) = -j\frac{e^2K_BT}{\pi\hbar^2(\omega-j2\Gamma)}\left(\frac{\mu_c}{K_BT}+2ln\left(e^{-\frac{\mu_c}{K_BT}}+1\right)\right) \qquad (3)$$

The letters Γ, K_B, ts, and $\hbar$ stand for the scattering rate, thickness, Boltzmann's constant, and Plank's constant, respectively, in eqn. (3). It is possible to alter "μc" by adjusting graphene's electric potential. Fig. 5 illustrates how the $|S_{11}|$ parameter is affected by the chemical potential of the graphene. It verifies that as graphene's "μc" increases, the working spectrum moves to higher frequencies.

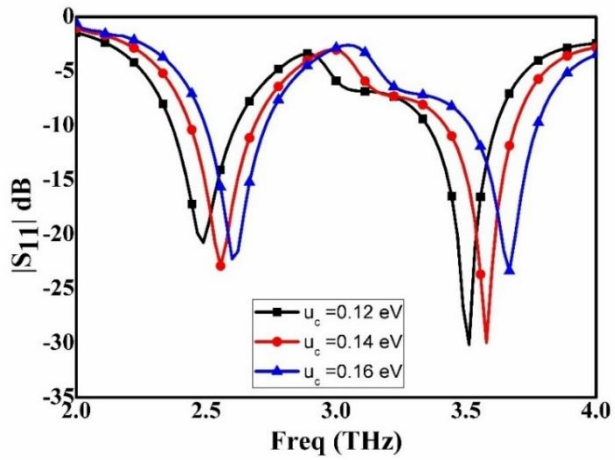


Fig. 5 $|S_{11}|$ graph with variation "μ_c"

Fig. 6 presents the S-parameter alteration with single and 2-terminal radiator. Two cases are taken in 2-terminal radiator i.e. with and without DGS. Two things are observed clearly: (i) $|S_{11}|$ parameter is not diverted after conversion from single terminal to 2-terminal; and (ii) DGS reduce the coupling value to below -25 dB in both the functioning regime.

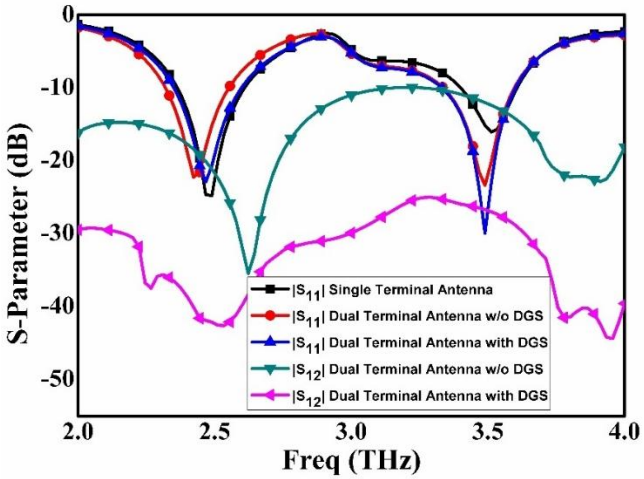


Fig. 6 S-parameter graph with single and dual terminal radiator

4. Prediction of $|S_{11}|$ using ML Approaches

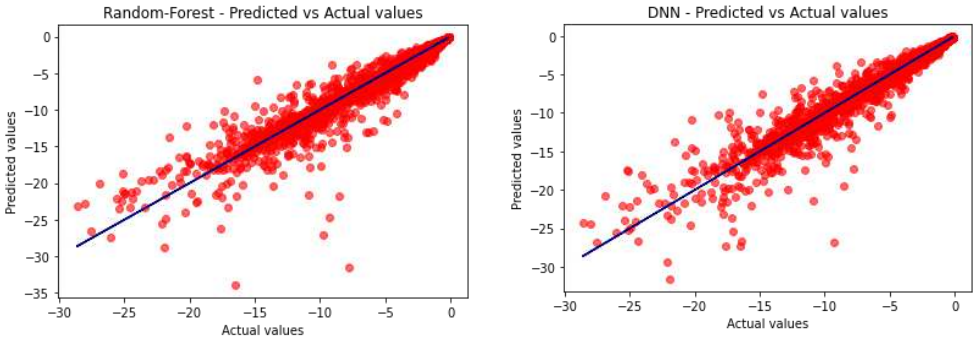
This section uses DNN and RF ML approaches to predict $|S_{11}|$. In order to do this, a data collection is created by varying a number of radiator settings within a particular series (data set). Both ML techniques are trained using this set of data. The sizes of several radiator limitations used to create the data set differ as follows:

- D varies in increments of 0.1µm between 14.0µm and 22.0µm
- H varies in increments of 0.1 µm between 6.0 µm and 12.0 µm.
- D1 varies in increments of 0.1µm between 1.0 µm and 4.0µm.
- L1 varies in increments of 0.1µm between 17.0 µm and 25.0 µm.
- W1 varies in increments of 0.1 µm between 1.0 µm and 4.0 µm.
- D5 varying between 1.0µm and 5.0µm in increments of 0.1µm;
- D3 fluctuating between 5.0 µm and 10.0 µm in steps of 0.1 µm;
- D4 fluctuating between 3.0 µm and 9.0 µm in steps of 0.1 µm

This data collection of |S11| was produced by the parametric assessment of the Ansys HFSS program. The frequency spectrum is 2.0–4.0 THz with a frequency point of 101. As a consequence, the whole dataset has around 125483 data points. The remaining 20% is set aside for evaluation, while the remaining 80% is utilized to master the ML approach. Three fundamental constraints—MAE, R2 score, and MSE—are used to assess the results of ML approaches [14]. Table 2 lists these numbers for DNN and RF. It is clear that ML approaches attain accuracy levels higher than 80%. It is regarded as a very good number. Additionally, it shows that DNN provides more accurate guesses than RF. Fig. 7 provides the charts comparing expected and actual results for RF and DNN built ML approaches. These figures demonstrate that the predicted and actual results for both ML approaches are almost equal. When the |S11| becomes close to 0 dB, the level of confidence is much higher.

Table-2 MSE/MAE/R2 score value for RF and DNN Approaches

ML Approaches	R2 Score (S11)	MSE (S11)	MAE (S11)
RF	0.931	4.025	0.745
DNN	0.857	3.559	0.815



(a) (b)

Fig. 7 Estimation Between real and predicted $|S_{11}|$ (a) RF (b) DNN

5. Final Outcomes

Using CST simulation software, the optimal results are confirmed in this part. |S11|/|S12| is the first antenna parameter to be confirmed. In Fig. 8, it is shown. A respectable association exists between |S11| and |S12|. The intended antenna has a coupling value of less than -25 dB and operates efficiently within two working regimes i.e. 2.2-2.65 THz and 3.3-3.7 THz. Fig. 9 shows the far-field pattern in XZ plane with terminal-1 and terminal-2 at 2.5 THz and 3.5 THz. It can be seen from Fig. 9 that broadsided pattern is got due to creation of fundamental hybrid mode. Similarly, co-pol has significantly large in comparison to cross-pol value, which confirms high efficiency of planned radiator.

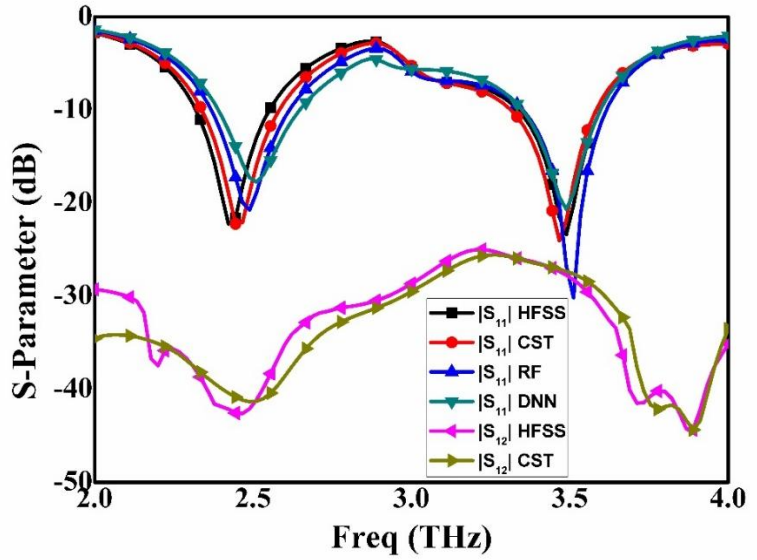


Fig. 8 Graph of S-parameter using HFSS/CST/ML Approaches

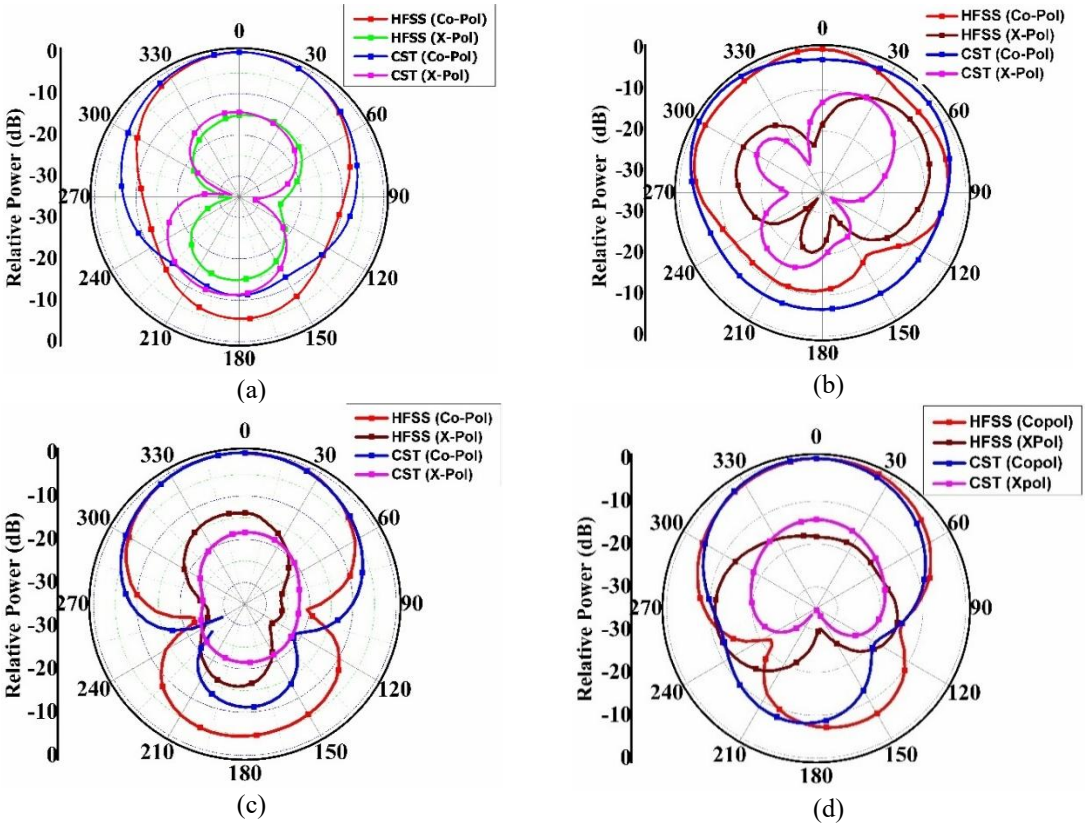


Fig. 9 Far-field pattern in XZ plane (a) 2.5 THz with Terminal-1 (b) 3.5 THz with Terminal-1 (c) 2.5 THz with Terminal-2 (d) 3.5 THz with Terminal-2

The alteration in gain generated by HFSS/CST for the suggested design is shown in Fig. 10. The HFSS and CST show excellent resemblance. The gain level is around 3.5 dBi and 4.5 dBi over the dual operational regime. The evaluation of the developed 2-terminal radiator in the THz regime in comparison to the published 2-terminal radiator in the same domain is listed in Table-3. This evaluation is based on gain level, coupling value, and impedance BW. It is evident from Table-3 that the plannned radiator is preferable in terms of each of the previously discussed metrics. Using machine learning to forecast the |S11| gives the planned radiator an extra advantage.

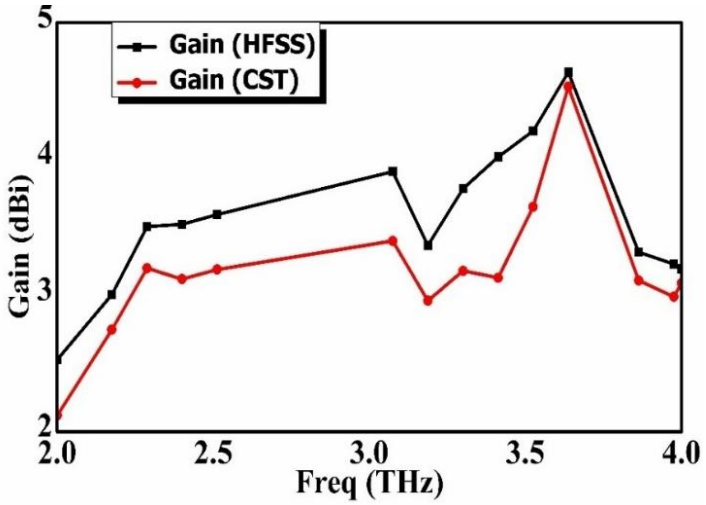


Fig. 10 Graph of Gain got from HFSS/CST

Table-3 Comparing planned radiator's ML optimization, isolation, and BW to the available 2-terminal radiator in THz region

Ref.	BW (THz)	Gain (dBi)	Coupling level (dB)	Estimate of $\|S_{11}\|$ via ML approaches
[5]	0.12	3.3	<-15	----
[6]	0.03	0.41	<-20	----
[7]	0.49	4.3	<-20	----
[8]	0.19	3.7	<-20	----
[9]	0.59	4.2	<-25	----
[10]	0.09	3.7	<-20	----
Planned Radiator	0.45/0.4	3.5/4.5	<-25	Yes

To determine its effectiveness in a fading context, two diversity parameters—ECC and DG—must now be examined. To make the closely spaced antennas uncorrelated, the ECC value should be small (less than 0.2). To be effective in a working context, the DG value should be high (around 10 dB) [18]. The ECC/DG change for the suggested radiator is shown in Fig. 11. It shows that the ECC and DG values are in good agreement with the CST/HFSS. While DG is around 10 dB throughout the operational range, ECC is much lower 0.2.

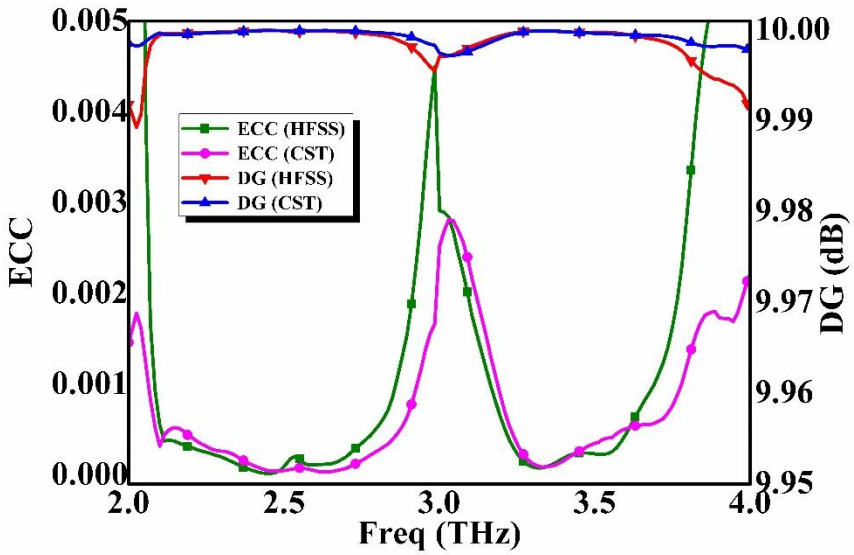


Fig. 11 Graph of ECC/DG got from HFSS/CST

6. Conclusion

A two-terminal radiator with band notch feature has been planned and examined in this communication. Modified ring slot fed ring dielectric rod provides wideband features i.e. 2.35-3.8 THz. Dual ring patches aligned on the both side of printed line adds band notch characteristics in between 2.75-3.15 THz. Due to dual orthogonal hybrid modes, the planned radiator functions in between 2.2-2.65 THz and 3.3-3.7 THz. Presence of DGS in between two terminal reduces the coupling level to below -25 dB. RF and DNN predicts the $|S_{11}|$ parameters accurately. All these features make the planned radiator appropriate for THz built mobile applications.

Declarations

***Ethics approval and consent to participate: Not Applicable**

*** Consent for publication: I, Pooja Singh, give my consent for the publication of identifiable details, which can include photograph(s) and/or videos and/or figures and/or details within the text ("Material") to be published in the above Journal and Article**

*** Availability of data and materials:** Not Applicable

*** Funding:** No funds, grants, or other support was received.

*** Authors' contributions:** Conceptualization and Methodology [Goutam Datta and Asha Verma]; Writing - revised draft preparation: [Neha K. Saini]; Analysis and Investigation: [Pooja Singh and Goutam Datta]; Writing - original draft preparation and Supervision: [Sreedhar Jadapalli]

*** Disclosure of potential conflicts of interest:** There are no potential conflicts of interest.

References

1. I.F. Akyildiz, J.M. Jornet, C. Han, "Terahertz band: next frontier for wireless communications" Phys. Commun., 12, 16-32 (2014)
2. M.A. Jensen and J.W. Wallace, "A review of antennas and propagation for MIMO wireless communications" IEEE Trans. Antennas Propagat., 52, 2810-2824, (2004)
3. A. Sharma, A. K. Dwivedi, N. K. Narayaswamy, Y. K. Prajapati, D. K. Tripathi, "Ceramic material-based optical antenna for multiband photonics applications" Optical Engineering, 61, 017104, (2022)
4. H.E. Misilmani, T. Naous and S.A. Khatib, "A Review on the Design and Optimization of Antennas Using Machine Learning Algorithms and Techniques" International Journal of RF and Microwave Computer-Aided Engineering, 30, 1-7 (2020)
5. G. Varshney, S. Gotra, V.S. Pandey and R.S. Yaduvanshi, "Proximity-coupled two-port multi-input-multi-output graphene antenna with pattern diversity for THz applications" Nano Commun Netw, 21, 100246-100253 (2019)
6. Q. Rubani, S.H. Gupta and A. Rajawat "A compact MIMO antenna for WBAN operating at Terahertz Frequency" Optik (Stuttg), 207, 164447-164454, (2020)
7. K.V. Babu, S. Das, G. Varshney, G.N.K. Sree and B.T.P. Madhav, "A micro-scaled graphene-based tree-shaped wideband printed MIMO antenna for terahertz applications" J Comput Electron, 21, 289–303 (2022)
8. C.S. Vamsi, A.K. Dwivedi, G. Bharti, V.R. Verma and A. Sharma, "Efficient graphene-based circularly polarized MIMO antenna for THz applications" Applied Optics, 61, 8155-8161 (2022)
9. Vishwanath, G. Varshney and B.C. Sahana, "Implementing the single / multiport tunable terahertz circularly polarized dielectric resonator antenna" Nano Commun Netw, 32, 100408 (2022)
10. M. F. Ali, R. Bhattacharya and G Varshney, "Graphene-based tunable terahertz self-diplexing/MIMO-STAR antenna with pattern diversity" Nano Communication Networks, 30, 100378-100386 (2021)
11. Z. Zheng, X. Chen and K. Huang, "Application of support vector machines to the antenna design," Int. J. RF Microw. Computer-Aided Eng., 21(1), 85-90 (2010)
12. Y. Sharma, H. Helen Zhang, and H. Xin "Machine Learning Techniques for Optimizing Design of Double T-shaped Monopole Antenna", IEEE Transactions on Antennas and Propagation, 68, 5658 – 5663 (2020)
13. P. Ranjan, A. Maurya, H. Gupta, S. Yadav, and A. Sharma "Ultra-Wideband CPW Fed Band-Notched Monopole Antenna Optimization Using Machine Learning" Progress in Electromagnetics Research M,108, 27–38 (2022)

14. A. Srivastava, H. Gupta, A. K. Dwivedi, K. K. V. Penmatsa, P. Ranjan and A. Sharma, “Aperture coupled dielectric resonator antenna optimization using machine learning techniques” AEU- International Journal of Electronics and Communications,154, 1-9 (2022)
15. G. Varshney, S. Gotra, J. Kaur, et al, “Obtaining the circular polarization in a nano-dielectric resonator antenna for photonics applications” Semicond Sci Technol, 34, 1–8 (2019)
16. D. Kajfez, A.W. Glisson and J. James, “Computed modal field distributions for isolated dielectric resonators”, IEEE Trans. Microw. Theory Tech., 32,1609-1616 (1984)
17. A. Sharma, G.Das and R.K. Gangwar, “Composite Antenna for Ultrawide Bandwidth Applications: Exploring Conceptual Design Strategies and Analysis” IEEE Antennas and Propagation Magazine, 60, 57-65, (2018)
18. M.S. Sharawi, “Current Misuses and Future Prospects for Printed Multiple-Input, Multiple-Output Antenna Systems [Wireless Corner]” IEEE Antennas Propag Mag, 59,162–170 (2017)